A New Fault Recognition Method Based on Empirical Mode Decomposition and Texture Attributes

Hui Qiao[1], Bingxin Chen[2,*], Yaping Huang[2], Xuemei Qi[2], Hongming Fan[3], Aiping Zeng[3]
[1]CHN Energy Yulin Energy CO., Ltd.,
Yulin 719000, China
[2]School of Resources and Geosciences, China University of Mining and Technology,
Xuzhou 221116, China
[3]Geophysical Prospecting and Surveying Team of Shandong Bureau of Coal Geology,
Jinan 250104, China
609761660@qq.com; [*]TS22010008A31@cumt.edu.cn; yphuang@cumt.edu.cn; qixuemei@cumt.edu.cn;
hmxwfhm@163.com; zaip626@sohu.com

***Abstract*—Small faults developed in coal seams are one of the major causes of coal mine accidents. Accurately predicting small faults in coal fields is an urgent requirement for efficient and safe production in coal mines. This article proposes a new small fault identification method that combines the empirical mode decomposition method and the seismic texture attribute extraction method to address the problem of large errors caused by noise in the results of small fault prediction. Firstly, the basic principles of the empirical mode method and the texture attribute method were studied, and then the fault recognition ability of this method was tested and analysed based on a small fault seismic forward modelling. Meanwhile, empirical mode decomposition is performed on actual seismic data to identify small faults by using texture attributes and by adding noise to the seismic record; this article compared the seismic record of texture properties in the presence and absence of noise. The results indicate that the texture attribute method can predict small faults well, but this method is easily disturbed by noise. The empirical mode decomposition method used in this paper can remove noise interference and highlight characteristics of the texture attribute. Therefore, the small fault prediction method that combines empirical mode decomposition with texture attributes can effectively identify small faults and play an important geological guarantee role in ensuring safe and efficient production in coal mines.**

***Index Terms*—Fault; Empirical mode decomposition; Texture attributes; Denoising.**

I. INTRODUCTION

At present, the geological results provided by the conventional 3D seismic exploration interpretation method cannot fully meet the requirements of coal mine safety and efficiency; especially the interpretation of the faults with more than 5 m is omitted, and even the interpretation of the faults above 10 m may deviate. The interpretation of the fault drop in the strata with large dip angle is greatly from the actual exposure, and the hidden geological anomalies in the coal seam cannot be effectively resolved. These problems have buried great safety risks for the safe and efficient production of coal mines. Therefore, finding small faults as soon as possible is conducive to improving the production capacity and benefit of the fully mechanised mining face of the coal mine, and also has positive guiding significance and practical value to ensure the safety production of the coal mine [1]–[3].

The seismic attribute is an effective method to identify small faults, but some commonly used seismic attribute methods in the past have limited accuracy for small faults with a drop of less than 5 m, so it is necessary to study a new seismic attribute method to improve the identification accuracy of small faults.

The identification accuracy of small faults is directly limited by the quality of the seismic data. Advanced data processing and denoising methods can improve the signal-to-noise ratio of seismic data to improve the quality of seismic data. Therefore, to improve the accuracy of small fault identification, it is necessary to study new and efficient data processing methods.

Research on the seismic texture attribute began in 1985. This year, Love and Siman officially introduced texture features into seismic exploration, and then many people continued to study deeply from this perspective and made certain achievements [4]–[6]. Lv and Huang [7] defined the two statistics of journey length and energy to analyse the image of the seismic profile. Monsen [8] introduced the watershed algorithm in the morphological field into the segmentation of the seismic profile image. Yan [9] combined the wavelet transform and the fractal waveform; this algorithm finally uses the iterative K-mean clustering method to segment the seismic profiles. Zhao [10] found a new method to extract texture features in the classification and identification of seismic profiles. The main idea of this new method is to use the best two-dimensional direction filtering ripple with the least energy loss. Song, Liu, Cai, Qian, and Hu

Manuscript received 28 August, 2024; accepted 11 December, 2024.
This research was supported by the National Natural Science Foundation of China under Grant No. 42274180; the National Key R&D Program of China under Grant No. 2021YFC2902003.

[11] have done a series of researches on the application of texture properties to seismic exploration. West, May, Eastwood, and Rossen [12] applied texture attribute to seismic phase classification. Zhang *et al.* [13] used an algorithm based on grayscale co-occurrence matrix to analyze three-dimensional seismic data. Matos, Yenugu, Angelo, and Marfurt [14] used the self-organisation mapping algorithm to process the seismic texture properties and apply them to the sand recognition. Hu, Chen, He, Huang, and Wen [15] used the fuzzy c-mean clustering algorithm to cluster and classify the extracted seismic texture properties, and applied them to the division of the seismic facies. Gong, Gui, Wang, Wang, and Zhang [16] and Gui, Yang, and Wang [17] applied texture attributes to the prediction of fissure.

Previous studies have proven the feasibility and effectiveness of small fault prediction methods with texture attributes. However, the texture attribute is greatly affected by noise, and most of the existing literature directly uses seismic data to extract the texture attribute and study the fault. Because the traditional denoising method will remove some effective signals while removing noise, this paper adopts the experience mode decomposition method to remove noise. Experience mode decomposition (EMD) is a time-frequency signal analysis method that can effectively decompose nonlinear signals. The time-frequency analysis method based on EMD has the advantages of intuitiveness, directness, posteriori, and self-adaptability, thus it is very suitable for the analysis [18]–[20] of nonlinear and nonstationary signals.

These scholars applied the texture attribute to the seismic field and made further improvement. Some scholars have used other methods to predict small faults and have also achieved good results. Zhang, Huang, Wu, and Dong [21] used azimuthal seismic data for ellipse fitting and achieved a good application effect in small fault prediction. Chen *et al.* [22] used the method of joint interpretation of pre-stack and post-stack seismic data to study the multi-scale fracture prediction method. Kaur, Zhang, Witte, Liang, Wu, and Fomel [23] carried out research on 3D fault identification of carbon capture and storage based on deep learning. Zeng Yan, Huang, Ren, Liu, and Zhang [24] used artificial intelligence methods to explain small faults. Gao [25] used 3D visualisation methods to interpret the faults. Shafiq, Wang, AlRegib, Amin, and Deriche [26].

applied texture attribute method to actual projects. Some scholars use other seismic properties to predict faults [27], [28].

Therefore, this paper proposes a method for small fault identification which uses a combination of mode decomposition and seismic texture attributes. First, we study the basic principles of the empirical modal method; then, we study the texture attributes to verify the denoising effect of the modal decomposition method and the identification ability of small faults. Finally, the example analysis shows that this method can accurately identify small faults and improve the accuracy of small fault identification.

II. The Basic Theory of Texture Attributes and Empirical Mode Decomposition

Extracting texture features is a very important step in texture analysis. At present, the common methods mainly include statistical methods, structural methods, model-based methods, and signal processing methods. Among them, the statistical method is one of the most widely used and representative methods. This paper mainly introduces the basic method principle of the grey-scale symbiotic matrix method of the statistical analysis method.

Grey symbiotic matrix is a texture attribute extraction method proposed by Haralick, Shanmugam, and I. Dinstein [29] in 1973. This method is a statistical method that describes the texture characteristics of an image by studying the correlation features of the spatial distribution of the grey level, namely by a statistical specific grey value in the number of times in a certain spatial location. It is based on the second-order combination condition, the probability of density function, and then the number of pixels in a specific direction, a specific distance condition, in order to achieve the purpose of generating matrix.

The principle of the grey-level co-occurrence matrix (GLCM) algorithm is as follows [4], [17].

The grey-scale symbiosis matrix is a matrix composed of the combined probabilities between the grey-scales of the two-dimensional data body. $[p(i,j,d,\theta)]_{M\times N}$, θ is the grey direction, L is the grey level, M is the row number of the grey symbiosis matrix, and N is the column number of the grey symbiosis matrix. Probability p is the probability of taking a point $G(x,y)$ with grey level of i as the starting point and the point $G(x+\Delta x, y+\Delta y)$ with grey value j the distance is d and the direction is θ.

The calculation equation of $p(i,j,d,\theta)$ is as follows

$$P(i,j,d,\theta)=\sum\left\{\begin{matrix}|G(x,y)=i,G(x+\triangle x,y+\triangle y)=\mathrm{j}\\ x=0,1,...M-1,y=0,1,...N-1\end{matrix}\right\}, \quad (1)$$

where $d=\sqrt{(\Delta x)^2+(\Delta y)^2}$, θ is usually selected with 0 °, 45 °, 90 °, and 135 °, $i=1,2...L-1$, $j=1,2...L-1$.

Figure 1 is a schematic representation of the grey-scale symbiosis matrix. Figure 1(a) is the grey value of the image, and Fig. 1(b) is the grey matrix of symbiosis (θ = 135 °).

2	1	2	0	1
0	2	1	1	2
0	1	2	2	0
1	2	2	0	1
2	0	1	0	1

(a)

	0	1	2
0	0	2	2
1	2	1	2
2	2	3	2

(b)

Fig. 1. Schematic representation of the grey-scale symbiosis matrix: (a) Image grey value; (b) Grey symbiosis matrix (θ = 135 °).

Because the grey-scale symbiosis matrix cannot clearly reflect the changes of the internal structural characteristics of the image, it is necessary to carry out the second statistics on the image data to make it a texture attribute with clear physical significance. The commonly used texture attributes based on the grey-scale symbiosis matrix are contrast, energy, entropy, and correlation. The formula is as follows.

1. Contrast attributes

$$C = \sum_{n=0}^{L-1} n^2 \left\{ \sum_{i=0}^{L-1} \sum_{j=0}^{L-1} P(i, j) \right\}. \quad (2)$$

Among them, $|i - j| = n$.

The contrast is also known as the moment of inertia near the main diagonal of the grey symbiosis matrix, which mainly reflects the distribution of the values in the matrix and the magnitude of local variation in the texture, reflecting the clarity of the texture. The higher the contrast, the sharper the image and the finer the texture, making the image easier to distinguish. If the amplitude changes in the seismic profile vary greatly, the elements of the amplitude symbiosis matrix are relatively small. If the value of the amplitude symbiosis matrix away from the diagonal is larger, the larger C is, the seismic image is deep, and the effect is clear. If the value of the element value away from the diagonal in the amplitude symbiosis matrix is smaller and the smaller the C, the seismic image is shallow and the effect is blurred.

2. Energy

$$E = \sum_{i=0}^{L-1} \sum_{j=0}^{L-1} P(i, j)^2. \quad (3)$$

The energy reflects the uniformity of the grey distribution of the image. It is a measure of whether the grey level of the texture changes evenly, reflecting the degree of uniformity and the thickness of the texture. If the energy value is large, the diagonal element value of the matrix will be large, which will lead to unclear image; otherwise, if the energy value is small, the grey level will change greatly, which will make the image clear.

3. Entropy

$$Ent = \sum_{i=0}^{L-1} \sum_{j=0}^{L-1} P(i, j) \log(P(i, j)). \quad (4)$$

Entropy measures the randomness of the amount of information that an image contains. Entropy is maximised when all values in the symbiosis matrix are equal, or when the entropy indicates the complexity of the grey distribution of the image. The larger the entropy, the more complex the image.

4. Correlation

$$Cor = \sum_{i=0}^{L-1} \sum_{j=0}^{L-1} \frac{ijP(i, j) - u_1 u_2}{\sigma_1^2 \sigma_2^2}, \quad (5)$$

where u_1 u_2 σ_1 σ_2 are, respectively,

$$u_1 = \sum_{i=0}^{L-1} i \sum_{j=0}^{L-1} P(i, j), \qquad u_2 = \sum_{i=0}^{L-1} j \sum_{j=0}^{L-1} P(i, j),$$

$$\sigma_1 = \sum_{i=0}^{L-1} (i - u_1)^2 \sum_{j=0}^{L-1} P(i, j),$$

$$\sigma_2 = \sum_{i=0}^{L-1} (i - u_2)^2 \sum_{j=0}^{L-1} P(i, j).$$

The correlation represents the degree of correlation of elements in the grey symbiosis matrix of the image in the direction of rows and columns of a matrix, and the distribution of grey values is related to the correlation of pairs of grey image elements. The more average the grey-scale distribution of the image, the better the correlation, the greater the value; otherwise, if the difference of image grey distribution is large, the correlation is worse, and the smaller the correlation value. Secondly, by comparing the magnitude of the grey value in different directions in the image, the correlation can also indicate the direction of the texture extension. If the difference between the grey value of the image in a certain direction and its grey value in other directions is very large, then the texture feature in this direction is stronger than that in other directions. For example, if the image has a horizontal texture, the image tends to be larger than the correlation value of the grey symbiosis matrix of $\theta = 0$ °. These texture metrics reflect the texture characteristics of the image from different sides, and there is some correlation between them.

There are four important parameters for the design of texture analysis using a grey symbiosis matrix: window size, movement direction, moving step length, and grey-scale level. The appropriate window size is particularly important for texture analysis. Although smaller windows can guarantee the homogeneity of pixels in the window, they cannot accurately and effectively describe the distribution regularity of various pixel arrangement. Although larger windows can guarantee representative texture statistics of similar objects, they may contain redundant information about different objects, which makes the pixels between different objects blurred. In short, different parameter settings build different grey-scale symbiosis matrices, and then obtain different texture attributes. Due to space limitations, this is not discussed here. The following parameters are used: the window size is 5×5, the grey-scale level is 16, and the moving step length is 1. After setting up the basic parameters, extract the texture attribute values from 4 directions (0°, 45°, 90°, 135°) at each sampling point, and their average values are the final texture attribute value.

Empirical mode decomposition (EMD) is a time-frequency signal analysis method that can effectively decompose nonlinear signals. EMD-based time-frequency analysis method has the advantages of intuition, direct, posterior, and adaptability, so it is very suitable for the analysis of nonlinear, nonstationary signals. The Hilbert yellow transformation (HHT) is divided into two steps, namely the signal empirical mode decomposition (EMD), the signal into a series of eigenmode functions (intrinsic mode function (IMF)), the decomposition signal Hilbert transformation, each component of the Hilbert spectrum, and finally all the Hilbert spectrum of the total Hilbert spectrum. To explain the EMD decomposition algorithm, we first introduce the concept of IMF. In the EMD decomposition, the IMF is defined as follows [18]–[20].

1. For the whole signal, there must be as many or at most one difference between the number of extreme points and the number of zero crosses.

2. At any time, from a local perspective, the mean of the upper envelope defined by the maximum point and the lower envelope defined by the minimum point is equal to zero, i.e., the upper and lower envelope of the signal is locally symmetric centred on the time axis.

The eigenmode function satisfies the monotone function condition, but most of the signals contain a series of signals with different frequency components, which does not meet the single component condition, especially the nonlinear nonstationary signals. Therefore, the purpose of the Hilbert yellow transformation is to decompose the signal, so that the signal can be decomposed into a series of monotonic functions from high-frequency to low-frequency arrangement, so as to perform the following Hilbert transformation.

The process of EMD decomposition is as follows.

The original signal $x(t)$ underwent cubic spline interpolation to calculate the mean envelope m_1. Subtracting m_1 with the original signal $x(t)$ yields a new data sequence, h_1

$$x(t) - m_1 = h_1. \tag{6}$$

Repeat the above process for h_1, with

$$h_1 - m_{11} = h_{11}. \tag{7}$$

where m_{11} is the mean of the upper and lower envelope of h_1. Repeat the appeal process k times until h_1k is a monotonic function, namely

$$h_1(k-1) - m_1k = h_1k. \tag{8}$$

The eigenmode function obtained from the first decomposition is expressed by c_1

$$c_1 = h_1k. \tag{9}$$

By extracting c_1 from the original signal $x(t)$, the remaining is the residual term r_1, namely

$$r_1 = x(t) - c_1. \tag{10}$$

Then, the residual term r_1 is used as the new sequence, and the above method is repeated to obtain the new residual term r_2, and then

$$r_2 = r_1 - c_2. \tag{11}$$

The above procedure is repeated until the residual term r_n is turned into a monotonic function. At the end of the signal decomposition, you get

$$x(t) = c_1 + c_2 + c_3 + ... + c_n + r_n. \tag{12}$$

In this way, the original signal is decomposed into n eigenmode functions and a residual term.

Through the above algorithm, the original signal is decomposed into multiple intrinsic mode functions (IMFs); by removing the interference signal and retaining the effective signal, the denoising through the EMD method is completed.

III. CALCULATION OF A MODEL

To verify the ability of texture attributes to identify faults, the seismic response characteristics of texture attributes to small faults were studied based on the fault model in [24]. The length of this geological model is 1000 m, mainly including loess, mudstone, and coal seam, the P wave velocity of the coal seam is 1600 m/s, with a density of 1.45 g/cm^3, the P wave velocity of the loess is 1800 m/s, with a density of 2.00 g/cm^3, and the P wave velocity of the mudstone is 2800 m/s, with the density of 2.30 g/cm^3, the small faults with a drop of 1 m, 3 m, 5 m, and 10 m were placed in the model at 200 m, 400 m, 600 m and 800 m respectively, the thickness of coal is 3.5 m. The forward simulation was conducted with the Ricker wave of 50 Hz, with a reception distance of 10 m and a total of 100 reception.

Based on these parameters, forward modelling was performed using the formulation of the convolution model of (13)

$$s(t) = r(t) * w(t). \tag{13}$$

where $r(t)$ is the sequence of reflection coefficients,

$$r = \frac{\rho_2 v_2 - \rho_1 v_1}{\rho_2 v_2 + \rho_1 v_1}, \tag{14}$$

$w(t)$ is the seismic wavelet sequence,

$$w = \left[1 - 2\left(\pi f_p t\right)^2\right] \exp\left[-\left(\pi f_p t\right)^2\right], \tag{15}$$

t is the two-way travel time of the reflected wave.

The seismic record is shown in Fig. 2.

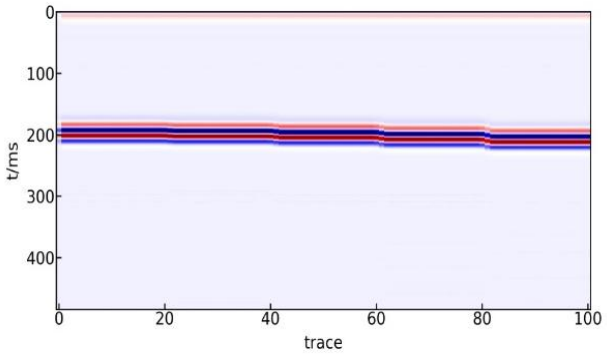

Fig. 2. Synthetic seismic record with different drop of fault model.

Texture attributes such as contrast, energy, entropy, and correlation of the grey symbiosis matrix were extracted, as shown in Figs. 2–6.

As can be seen from Fig. 3, the contrast attributes of the grey symbiosis matrix reflect the clarity of the texture. Figures 3(a) to 3(d) show contrast texture attributes at 0 °, 45 °, 90 °, and 135 °, respectively. The deeper the groove of

the texture, the greater the contrast, and the better the visual clarity of the image. That is, if the difference between the seismic data value is large, the element of the grey symbiosis matrix is relatively small, and the larger the element value away from the diagonal line in the grey symbiosis matrix, the greater the C, the seismic image is deep and the effect is clear. On the contrary, if the difference of seismic data is small, the elements of the grey symbiosis matrix are relatively large and the contrast is smaller.

Due to the fault of the same phase axis of the reflected wave at the fault, the deformation leads to the amplitude in the fault, and the change difference of the amplitude point becomes larger, making each element of the grey-scale symbiosis matrix relatively small, so the contrast value at the fault point is relatively large. As can be seen in Fig. 3, the fault value is red, which is one of the seismic response characteristics of the identified fault.

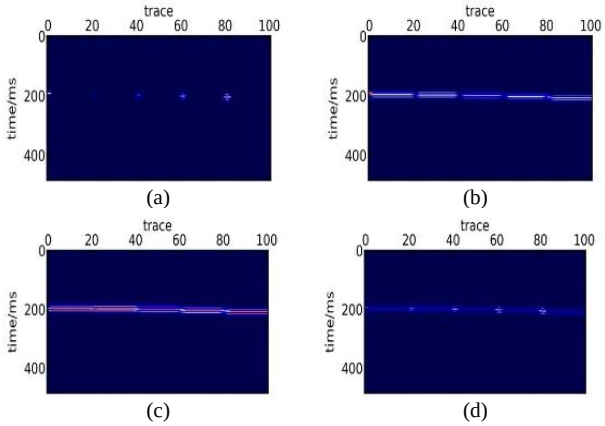

Fig. 3. Contrast texture attributes: (a) 0 °; (b) 45 °; (c) 90 °; (d) 135 °.

Figures 4(a) to 4(d) show the energy texture attributes at 0 º, 45 º, 90 º, and 135 º, respectively. As shown in Fig. 4, the energy of the grey-scale symbiosis matrix is the sum of squares of the elements of the amplitude symbiosis matrix, indicating the uniformity of the grey-scale distribution, where the higher energy reflects the coarse texture and the lower energy reflects the fine texture. If the amplitude value of the seismic data changes greatly, the elements of the grey symbiosis matrix are relatively small, then the value is small; otherwise, when the difference of the seismic data is small, some elements of the grey symbiosis matrix are relatively large and the value is large. Larger values indicate more uniform and regular texture patterns. As can be seen in Fig. 4, the boundaries and faults of the stratum are all dark blue with small values.

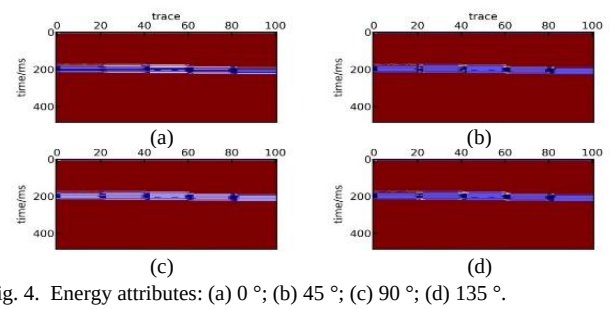

Fig. 4. Energy attributes: (a) 0 °; (b) 45 °; (c) 90 °; (d) 135 °.

Figures 5(a) to 5(d) show the entropy texture attributes at 0 º, 45 º, 90 º, and 135 º, respectively. The entropy of the grey-scale symbiosis matrix measures the randomness of the information contained in the image. The entropy value indicates the complexity of the image grey-scale distribution. The larger the entropy, the more complex the image. In the small fault area, the geological structure is complex, the entropy value is large, and there are obvious responses in all four directions.

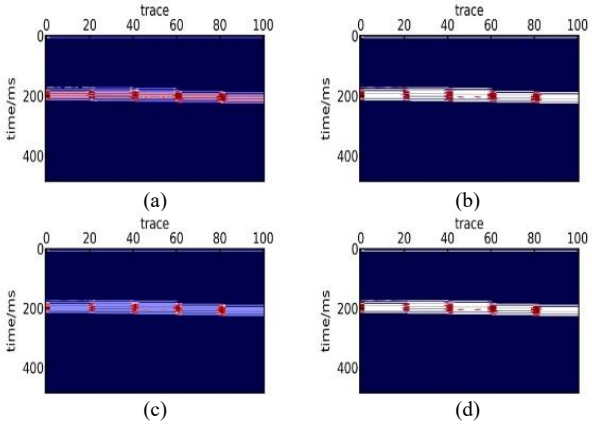

Fig. 5. Entropy attributes: (a) 0 °; (b) 45 °; (c) 90 °; (d) 135 °.

Figures 6(a) to 6(d) show the texture attributes of the correlation at 0 º, 45 º, 90 º, and 135 º, respectively. Correlation represents the degree of correlation of elements in grey-scale symbiosis matrix in the row direction and column direction of a matrix, which reflects the extension length of the grey value in a certain direction, and the longer the spread, the average the distribution of the grey symbiosis matrix; on the other hand, if the larger the grey distribution of the image, the worse the correlation, the smaller the correlation value.

In coalfield seismic exploration, faults with a drop of less than 3 meters are generally defined as small faults. The geological model designed includes fault drops of 1 m, 3 m, 5 m, and 10 m, and four texture attributes that have a certain response at the fault, which can be used to infer the location of the fault. In conclusion, a comparative analysis of the four texture attributes of the small fault seismic model shows that all the four texture attributes correctly highlight small faults in prominent geological structures in the ideally noiseless synthetic seismic records.

To test the effect of noise on texture attributes, a random noise with signal-to-noise ratio of five was added to the synthetic seismic record shown in Fig. 2. The noise is artificially added, and its frequency and waveform are very different from seismic waves, which has a great influence on the prediction accuracy. As shown in Fig. 7, due to the influence of noise, the fault does not show up well on the seismic profile, and noise has a great effect on small faults so that the fault almost cannot be noticed. Figures 8(a) to 8(d) show contrast texture attributes at 0 º, 45 º, 90 º, and 135 º, respectively. Due to the influence of noise, the fault with the drop of 1 m or 3 m received great interference in contrast texture attributes, so it could not be recognised effectively, while the fault with a drop of 5 m and 10 m has a certain response, but the characteristics are not obvious. The comparison results with the geological model fault settings show that the 0 ° ratio texture attribute has a better fault discrimination effect among the contrast attributes of the four

angles.

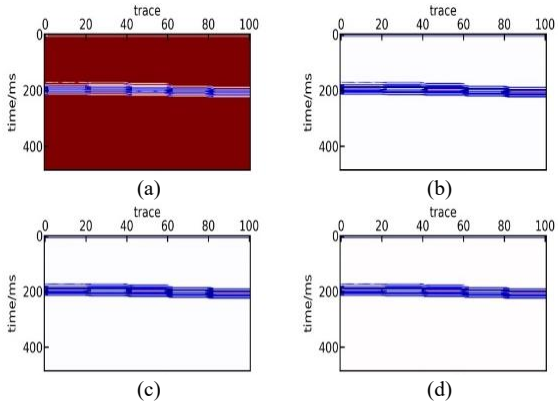

Fig. 6. Correlation attributes: (a) 0 °; (b) 45 °; (c) 90 °; (d) 135 °.

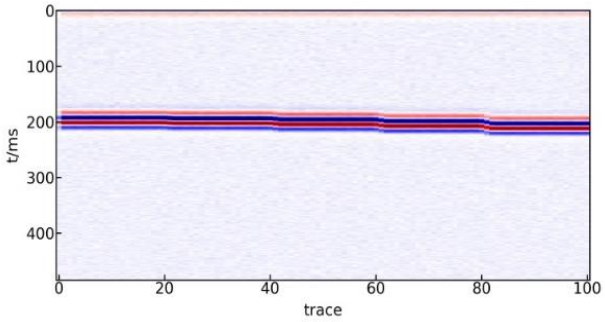

Fig. 7. Synthetic seismogram after adding noise.

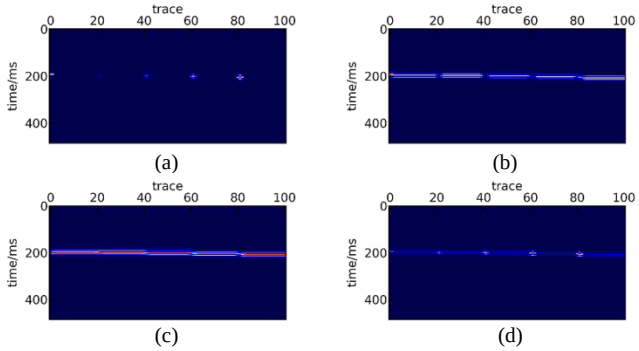

Fig. 8. Contrast attributes of the grey-scale symbiosis matrix with synthetic noise seismic records: (a) 0 °; (b) 45 °; (c) 90 °; (d) 135 °.

EMD is a method that can effectively carry out signal decomposition, after which the noise can be effectively removed. Therefore, the EMD method is first used to decompose Fig. 7 to obtain the IMF component shown in Fig. 9, in which the signal frequency in IMF1(Fig. 9(a)) is high and the main component is random noise; IMF2 (Fig. 9(b)) and IMF3 (Fig. 9(c)) are mainly active components of seismic signal, and IMF4 (Fig. 9(d)) is the residual trend of the signal. Therefore, add IMF2 and IMF3 to obtain the synthetic seismography profile after effectively denoising, and calculate the contrast attributes of the grey-scale symbiosis matrix as shown in Figs. 10(a)–10(d) at 0 °, 45 °, 90 °, and 135 °, respectively. Due to the more effective denoising processing, the faults of 1 m drop can see a more fuzzy response, while the faults of 3 m, 5 m, and 10 m have a more obvious response in contrast texture attributes, which is conducive to the identification of faults. Similarly, of the four-angle contrast texture attributes. The ratio of 0 ° texture attributes can effectively identify the location of breakpoints, and the texture attributes of other angles can be used to depict features such as fault inclination.

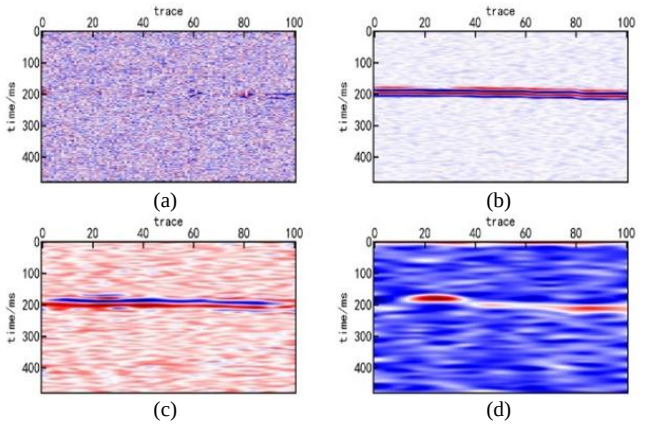

Fig. 9. EMD decomposition results for noise synthesis seismic records: (a) IMF1; (b) IMF2; (c) IMF3; (d) IMF4.

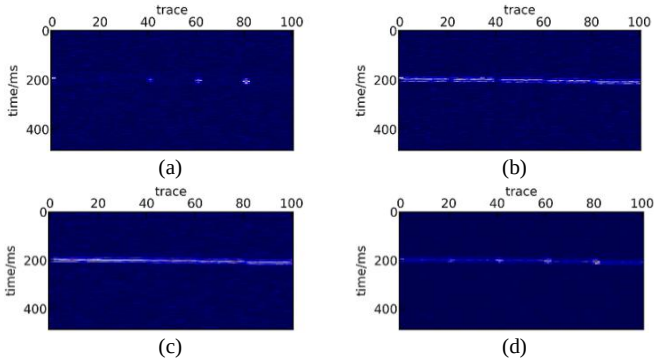

Fig. 10. Contrast attributes of the grey symbiosis matrix for denoised synthetic seismic records: (a) 0 °; (b) 45 °; (c) 90 °; (d) 135 °.

However, when there is noise in seismic profiles, texture attributes such as energy, entropy, and correlation also have response characteristics with the contrast texture attribute type. Therefore, in the process of extracting the texture attributes of the actual seismic data, it is necessary to denoise the seismic data first, and then extract the texture seismic attributes, which is more conducive to the identification and control of faults.

The EMD denoising method can effectively remove noise and retain an effective seismic signal, which can improve the signal-to-noise ratio of seismic data. Compared with seismic data without denoising, the quality of seismic data after EMD denoising is higher, the abnormal features on seismic profiles are very obvious, and the interference is less. Moreover, the contrast texture properties extracted from the de-noising seismic data are more obvious and can clearly reflect the small faults. Therefore, the EMD denoising method is conducive to the accurate identification of small faults.

IV. Application Examples

The study area is located in the northeast of the Ordos Basin, and the exposed and drilled strata in the well field are old to new: the Mesozoic Triassic Upper System Extension Formation (T_3y), Jurassic Lower Group (J_1f), Jurassic Middle Yan'an Group (J_2y), Xin Tong Bao de Group (N_2b), Lishi Group (Q_2l), and Holocene series (Q_4). The coal-bearing formation in the well field is the Middle Jurassic Yan'an Formation, which is divided into three coal-bearing sections from bottom to top, with each section containing one coal group, numbered 3,4, and 5 coal groups. The faults studied in

this study were mainly located in the 5-1 coal seam. The coal seam is located at the top of the first section of the Yan'an Formation, and the upper distance from the 4-3 coal seam is 27.30 m~63.60 m. The coal seam is 51.48 m on average, generally 46 m~57 m, distributed throughout the well field and all recoverable. This coal seam is also the main coal seam produced in the research area. Therefore, the study of the distribution and development of small coal seams plays an important role in ensuring the safe and efficient production of the coal mine.

Figure 11 shows the Inline621 seismic profile for this area. Therefore, the response characteristics of the coal seam in this area are obvious, which is conducive to the identification and characterisation of the coal seam. According to the previous manual explanation, there are F1, F2, and F3 faults in this section.

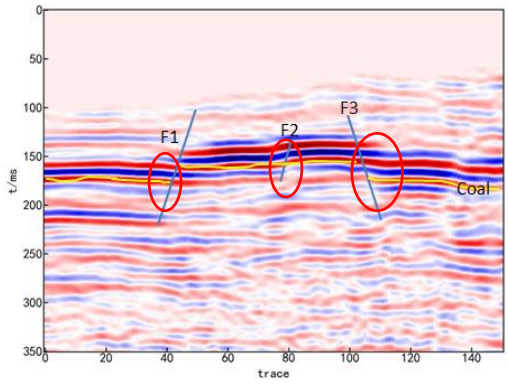

Fig. 11. Inline621 seismic profile.

The basic information for each fault is as follows.

F1 fault: positive fault, its direction is NW, its tendency is SW, inclination 60 °~70 °, drop about 0 m~28 m, from the northwest into the area, tip in the exploration area, the extension length of the area is about 2100 m. There are 104 rating breakpoints, including 63 class A breakpoints, 31 class B breakpoints, and 10 class C breakpoints, which are reliable faults.

F2 fault: positive fault, located at the northwest boundary of the survey area. It is a newly discovered fault. The fault approaches NWW to SSW with an inclination of 60 °, drop about 0 m~3 m and extension length approximately 140 m.

F3 fault: positive fault, located in the central and northern part of the survey area, the fault is NW, NE, the inclination is 60 °~70 °, the drop is about 30~70 m, running through the whole area, and the extension length of the area is about 3800 m. There are 187 rating breakpoints, including 118 A breakpoints, 56 B breakpoints, and 13 grade C breakpoints, which are reliable faults.

The drop in F1 and F2 is large, which is easy to identify in the seismic profile, while the drop in the F2 fault is only about 3 m, so the response characteristics in the seismic profile are not obvious. According to Section III, effectively denoising seismic profiles and then extracting texture attributes facilitate the identification and analysis of small faults. Therefore, the Inline621 seismic profile is denoised, and the seismic profile shown in Fig. 12 is obtained. Figures 12(a) to 12(d) show the IMF1, IMF2, IMF3, and IMF4 of the Inline621 seismic data, respectively.

After empirical mode decomposition, the seismic signal is decomposed into four parts, and the effective signal and part of the noise are separated. Using the effective seismic signal for subsequent analysis can greatly reduce the uncertainty in the prediction of a small fault. The resolution of the seismic data is effectively improved, which is conducive to the extraction of texture attributes and the identification of small faults.

The contrast texture attributes are extracted from the denoised seismic data, and the results are shown in Fig. 13. Based on the contrast texture attributes of the denoised seismic profile and the comparison with the original seismic record, it showed that the contrast texture attribute can effectively depict the fault, the 0 ° texture attribute can reflect the breakpoint position of the fault well, while the other three angles texture attribute can describe the fault characteristics more accurately. Through the analysis of the texture attributes of the four angles, the location of the fault can determine the region shown by the oval in Fig. 13. Other texture attributes also have response features that are generally consistent with contrast texture attributes and are not explained in detail here of length.

Compared to the seismic profile and the texture attributes of the seismic profiles, F2, a small fault that is difficult to identify in the seismic profile, has obvious features in the texture attributes of the seismic profiles, so in the application of actual data, texture attributes can effectively identify small faults.

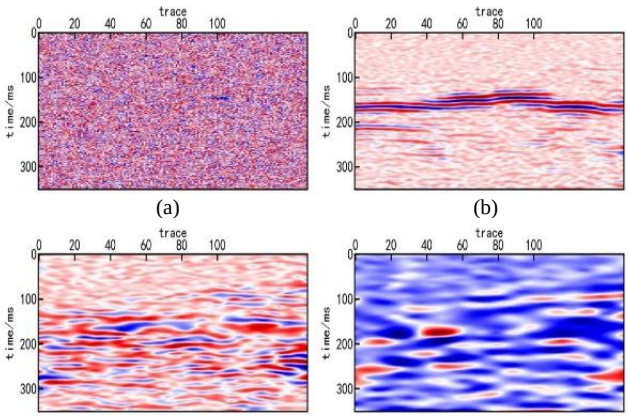

Fig. 12. Inline621 seismic profile decomposition results: (a) IMF1; (b) IMF2; (c) IMF3; (d) IMF4.

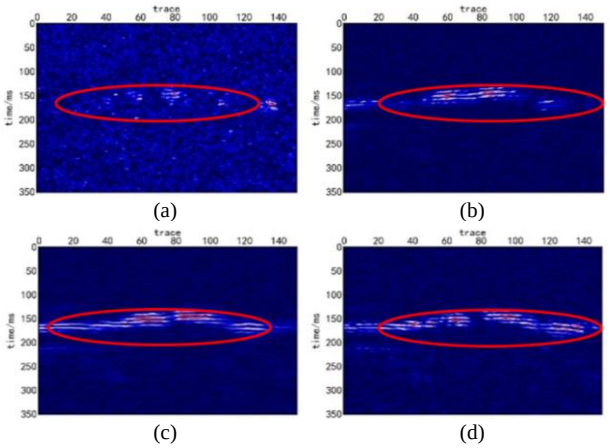

Fig. 13. Inline621 Contrast texture attributes of seismic profiles: (a) 0 °; (b) 45 °; (c) 90 °; (d) 135 °.

In summary, in the identification of small faults in seismic data, it is of great significance to extract various texture

attributes based on EMD denoising, which can effectively identify small faults and ensure the safe production of the coal mine.

V. CONCLUSIONS

1. The empirical mode decomposition is very suitable for the analysis of seismic data. Using this method, noise interference can be removed, the effective seismic signal can be retained, and the accuracy of small fault prediction can be improved.
2. After effectively removing noise effects, texture properties can well depict small faults.
3. In contrast to texture attributes of the four angles, 0^{o} texture attributes can effectively identify the breakpoint position, and other pairs of texture attributes can be used to depict the fault inclination. Therefore, the contrast texture attributes can effectively judge the existence of small faults and characterise their morphology.
4. When extracting a texture attribute, the window, step length, angle, grey-scale layer, and other settings also have an impact on the results of the texture attributes. Subsequently, it is still necessary to study each parameter to further improve the effect of texture attributes in predicting small faults.

CONFLICTS OF INTEREST

The authors declare that they have no conflicts of interest.

REFERENCES

[1] F. Pourahmadian and B. B. Guzina, "On the elastic anatomy of heterogeneous fractures in rock", *International Journal of Rock Mechanics and Mining Sciences*, vol. 106, pp. 259–268, 2018. DOI: 10.1016/j.ijrmms.2018.04.011.

[2] W. F. Du and S. P. Peng, "Prediction of small faults in coal seam by using curvature of seismic layer", *Chinese Journal of Rock Mechanics and Engineering*, vol. 27, pp. 2901–2906, 2008.

[3] T. Lohr *et al.*, "Prediction of subseismic faults and fractures: Integration of three-dimensional seismic data, three-dimensional retro-deformation, and well data on an example of deformation around an inverted fault", *AAPG Bulletin*, vol. 92, no. 4, pp. 473–485, 2008. DOI: 10.1306/11260707046.

[4] S. Cui, J. Zhang, W. Wang, M. Tan, and H. Chen, "The extraction of seismic texture attribute and its application in fault identification", *Computing Techniques for Geophysical and Geochemical Exploration*, vol. 32, no. 3, pp. 304–309, 2010. DOI: 10.3969/j.issn.1001-1749.2010.03.014.

[5] A. A. Aqrawi, T. H. Boe, and S. Barros, "Detecting salt domes using a dip guided 3D Sobel seismic attribute", in *SEG Technical Program Expanded Abstracts*, 2011, pp. 1014–1018. DOI: 10.1190/1.3627377.

[6] A. Berthelot, A. H. S. Solberg, E. Morisbak, and L.-J. Gelius, "Salt diapirs without well defined boundaries – A feasibility study of semi-automatic detection", *Geophysical Prospecting*, vol. 59, no. 4, pp. 682–696, 2011. DOI: 10.1111/j.1365-2478.2011.00950.x.

[7] Z. X. Lv and Z. L. Huang, "Image optimal neighborhood adaptive smoothing technique", *Computer Systems & Applications*, vol. 7, no. 7, pp. 40–41, 1998.

[8] E. R. Monsen, "Iron nutrition and absorption: Dietary factors which impact iron bioavailability", *Journal of the American Dietetic Association*, vol. 88, no. 7, pp. 786–790, 1988. DOI: 10.1016/S0002-8223(21)07902-5.

[9] X. L. Yan, "Fractal dimension analysis and its application in seismic section image segmentation", Ph.D. dissertation, Nanjing University of Science and Technology, 2004.

[10] R. C. Zhao, "A new method for extraction and segmentation of image texture features", *Acta Electronica Sinica*, vol. 22, no. 4, pp. 46–52, 1994. DOI: 10.3321/j.issn:0372-2112.1994.04.008.

[11] C.-Y. Song, Z.-N. Liu, H.-P. Cai, F. Qian, and G.-M. Hu, "Pre-stack-texture-based reservoir characteristics and seismic facies analysis", *Applied Geophysics*, vol. 13, no. 1, pp. 69–79, 2016. DOI: 10.1007/s11770-016-0541-5.

[12] B. P. West, S. R. May, J. E. Eastwood, and C. Rossen, "Interactive seismic facies classification using texture attributes and nerves Network", *The Leading Edge*, vol. 21, no. 10, pp. 945–1064, 2002. DOI: 10.1190/1.1518444.

[13] M. Zhang *et al.*, "Visual morbidity due to inaccurate spectacles among school children in rural China: The See Well to Learn Well Project, report 1", *Investigative Ophthalmology & Visual Science*, vol. 50, no. 5, pp. 2011–2017, 2009. DOI: 10.1167/iovs.08-2849.

[14] M. C. de Matos, M. Yenugu, S. M. Angelo, and K. J. Marfurt, "Integrated seismic texture segmentation and cluster analysis applied to channel delineation and chert reservoir characterization", *Geophysics*, vol. 76, no. 5, pp. 1SO–Z122, 2011. DOI: 10.1190/geo2010-0150.1.

[15] Y. Hu, H. Chen, Z. H. He, D. J. Huang, and X. T. Wen, "Seismic facies classification based on seismic texture attributes and fuzzy clustering", *Oil Geophysical Prospecting*, vol. 48, no. 1, pp. 114–120, 2013. DOI: 10.13810/j.cnki.issn.1000-7210.2013.01.018.

[16] Y. Gong, Z. X. Gui, P. Wang, Y. Wang, and C. Zhang, "Fracture distribution prediction based on seismic texture attribute clustering analysis", *Science, Technology and Engineering*, vol. 17, no. 30, pp. 167–174, 2017.

[17] Z. Gui, X. Yang, and P. Wang, "Fracture prediction method based on seismic texture attribute and its application", *Journal of Yangtze University (Natural Science Edition)*, vol. 20, no. 3, pp. 33–39, 2023. DOI: 10.16772/j.cnki.1673-1409.20220311.001.

[18] N. E. Huang, Z. Shen, and S. R. Long, "A new view of nonlinear water waves: The Hilbert spectrum", *Annual Review of Fluid Mechanics*, vol. 31, no. 1, pp. 417–457, 1999. DOI: 10.1146/annurev.fluid.31.1.417.

[19] J.-H. Cai, J.-T. Tang, X.-R. Hua, and Y.-R. Gong, "An analysis method for magnetotelluric data based on the Hilbert-Huang Transform", *Exploration Geophysics*, vol. 40, no. 2, pp. 197–205, 2009. DOI: 10.1071/EG08124.

[20] Z. Wu and N. E. Huang, "Ensemble Empirical Mode Decomposition: A noise-assisted data analysis method", *Advances in Adaptive Data Analysis*, vol. 1, no. 1, pp. 1–41, 2009. DOI: 10.1142/S1793536909000047.

[21] L. Zhang, Y. Huang, B. Wu, and S. Dong, "Identifying minor faults on top of coalfield Ordovician limestone stratum using seismic attributes derived from azimuthally tacked data", *Interpretation*, vol. 10, no. 3, pp. 1A–T580, 2022. DOI: 10.1190/INT-2021-0250.1.

[22] G. Chen *et al.*, "Multi-scale fracture prediction of shale oil reservoir driven by the combination of post-stack and pre-stack seismic data", *Chinese Journal of Geophysics*, vol. 67, no. 7, pp. 2830–2849, 2024. DOI: 10.6038/cjg2023Q0910.

[23] H. Kaur, Q. Zhang, P. Witte, L. Liang, L. Wu, and S. Fomel, "Deep-learning-based 3D fault detection for carbon capture and storage", *Geophysics*, vol. 88, no. 4, pp. 1JA–V359, 2023. DOI: 10.1190/geo2022-0755.1.

[24] A. Zeng, L. Yan, Y. Huang, E. Ren, T. Liu, and H. Zhang, "Intelligent detection of small faults using a support vector machine", *Energies*, vol. 14, no. 19, p. 6242, 2021. DOI: 10.3390/en14196242.

[25] D. Gao, "Volume texture extraction for 3D seismic visualization and interpretation", vol. 68, no. 4, pp. 1126–1422, 2003. DOI: 10.1190/1.1598122.

[26] M. A. Shafiq, Z. Wang, G. AlRegib, A. Amin, and M. Deriche, "A texture-based interpretation workflow with application to delineating salt domes", *Interpretation*, vol. 5, no. 3, pp. 1A–T449, 2017. DOI: 10.1190/INT-2016-0043.1

[27] J.-G. Song, Y.-Z. Sun, and D.-Z. Ren, "Edge detection technique based on structure-directed gradient attribute", *Chinese Journal of Geophysics*, vol. 56, no. 10, pp. 3561–3571, 2013. DOI: 10.6038/cjg20131031.

[28] Z.-x. Gui, T.-y. Duan, Y.-y. Yi, and H.-g. Xu, "On P-wave seismic detection methods for fractured reservoirs", *Journal of Oil and Gas Technology*, vol. 29, no. 4, pp. 75–79, 2007.

[29] R. M. Haralick, K. Shanmugam, and I. Dinstein, "Textural features for image classification", *IEEE Transactions on Systems, Man, and Cybernetics*, vol. SMC-3, no. 6, pp. 610-621, 1973. DOI: 10.1109/TSMC.1973.4309314.